Available online at www.sciencedirect.com
SCIENCE DIRECT
Physics of the Earth and Planetary Interiors 156 (2006) 75–88
PHYSICS OF THE EARTH AND PLANETARY INTERIORS
www.elsevier.com/locate/pepi

Lattice preferred orientation in deformed polycrystalline (Mg,Fe)O and implications for seismic anisotropy in D″

Maureen D. Long [a,*], Xiaohui Xiao [a], Zhenting Jiang [b], Brian Evans [a], Shun-ichiro Karato [b]

[a] *Department of Earth, Atmospheric, and Planetary Sciences, Massachusetts Institute of Technology, 77 Massachusetts Ave., Cambridge, MA 02139, United States*

[b] *Department of Geology and Geophysics, Yale University, P.O. Box 208109, New Haven, CT 06520, United States*

Received 29 June 2005; received in revised form 11 January 2006; accepted 3 February 2006

Abstract

Magnesiowüstite [(Mg,Fe)O] is an important constituent of the lower mantle, probably occupying about 20–25% of its volume. Laboratory and theoretical studies have shown this mineral to be highly elastically anisotropic at lower mantle pressures and temperatures. Thus, strain-induced formation of lattice preferred orientation (LPO) in magnesiowüstite is a candidate mechanism for the origin of anisotropic structure in D″. Although observations of seismic anisotropy within D″ are robust, both the occurrence and the style of that anisotropy are spatially variable. Two hypotheses have been offered to explain the observations of D″ anisotropy: LPO of intrinsically anisotropic minerals, or shape preferred orientation (SPO), perhaps in the form of horizontal layering or oriented inclusions. To investigate the first hypothesis, we performed confined simple shear deformation experiments in the dislocation creep regime using a gas-medium deformation apparatus over a range of compositions: the MgO and FeO endmembers and three intermediate compositions. Samples were deformed at 1273–1473 K, at a confining pressure of 300 MPa, to large shear strains ($\gamma = 3.5$–4.5) using deformation pistons cut at 45°. After deformation, the LPO was measured by electron backscatter diffraction (EBSD). The LPO produced varied for differing compositions, indicating the activity on individual slip systems and/or the nature of grain boundary migration in (Mg,Fe)O are affected by composition and/or homologous temperature. We predicted seismic anisotropy from the measured LPOs and theoretically determined single-crystal elastic constants. Anisotropic behavior predicted from LPO agrees well with observations of D″ anisotropy, so the LPO hypothesis appears to satisfy the seismological constraints. Our calculated anisotropy patterns suggest that if D″ anisotropy is due to LPO of (Mg,Fe)O, then azimuthal variations in anisotropy in the horizontal plane should be present. Such azimuthal variations are not generally predicted for SPO-type hypotheses, and this may provide a means for distinguishing the cause of D″ anisotropy.

Keywords: D"; Anisotropy; Deformation; Lattice preferred orientation; S-wave splitting

1. Introduction

The D″ layer comprises the bottom 150–300 km of the Earth's mantle and is characterized by unusually small vertical gradients in seismic velocity, laterally heterogeneous velocity structure, and probably by significant thermal and/or chemical heterogeneities (see Wysession

* Corresponding author. Tel.: +1 617 253 3589; fax: +1 617 258 9697.
E-mail address: mlong@mit.edu (M.D. Long).

0031-9201/$ – see front matter © 2006 Elsevier B.V. All rights reserved.
doi:10.1016/j.pepi.2006.02.006

et al., 1998, for a review). An understanding of the properties and dynamical processes associated with the core–mantle boundary (CMB) is essential to unravel the nature of mantle convection and coupling between the mantle and the core. To date, seismological observations have provided the strongest constraints on the nature of D″, and among the most important of these have been observations of seismic anisotropy. Although most of the lower mantle appears to be isotropic, at least on the scale of seismic wavelengths (e.g. Meade et al., 1995), several studies have suggested various styles of anisotropy in D″, beginning with Mitchell and Helmberger (1973), Doornbos et al. (1986), and Cormier (1986). Because anisotropic structures in the Earth's mantle are thought to result from permanent strain, observations of seismic anisotropy in D″ can provide useful insights into deformation geometry.

Although there is ample seismological evidence for anisotropy in D″, it appears that neither the style of anisotropy nor its spatial distribution is uniform. In studies of D″ anisotropy using core-diffracted shear waves (S_{diff}), Vinnik et al. (1989, 1995, 1998) have noted splitting of S_{diff} and anomalously high SV_{diff} amplitudes and suggested that elastic anisotropy was responsible. Observations of splitting in pre-diffracted *S* phases turning in the lowermost mantle have been interpreted in terms of transverse isotropy (that is, hexagonal symmetry with a vertical symmetry axis). Beneath the northern Pacific and Alaska (Lay and Young, 1991; Matzel et al., 1996; Garnero and Lay, 1997; Fouch et al., 2001), North America and the Caribbean (Kendall and Silver, 1996; Garnero and Lay, 2003), and the Indian Ocean (Ritsema, 2000), there is evidence for anisotropy in D″, apparently with a vertical axis of symmetry. Beneath the southern Pacific, it appears that the lowermost mantle is isotropic, while beneath the central Pacific there is evidence for highly spatially variable anisotropy, possibly with a horizontal axis of symmetry (that is, azimuthal anisotropy) (Lay et al., 1998). These spatial distributions of anisotropy have led to speculation that the mechanisms of anisotropy generation differ in regions associated with mantle upwelling and downwelling (Kendall, 2000).

In the upper mantle, it is generally accepted that seismic anisotropy results from lattice preferred orientation (LPO) produced by dislocation creep of olivine, the major upper mantle constituent (e.g. Zhang and Karato, 1995). Two different mechanisms for generation of anisotropy in D″ have been proposed. First, LPO of anisotropic lower mantle minerals could result in D″ anisotropy (Karato, 1998a,b), provided that deformation occurs by dislocation creep, rather than diffusion creep (see, for example, Karato, 1989). The observation that the lower mantle is largely isotropic has been interpreted as evidence that the dominant deformation mechanism is diffusion creep or superplasticity (Karato et al., 1995). However, recent geodynamical models (McNamara et al., 2001, 2002) have shown that dislocation creep may occur in the lowermost mantle, due to high stresses associated with the collision of subducted slabs with the CMB.

A second hypothesis suggests that anisotropy in D″ might result from shape preferred orientation (SPO) of inclusions within a matrix of differing elastic properties. For example, Kendall and Silver (1998) considered models consisting of oriented cigar-shaped or disk-shaped inclusions, due to the infiltration of core material or partial melting, and of horizontal layering, due to the presence of a subducted slab "graveyard." These workers concluded that SPO could explain the seismological data well. The SPO mechanism has also been considered by Russell et al. (1998), Garnero and Lay (2003), and Moore et al. (2004). Consensus on which model for anisotropy best explains the seismic data and available dynamical constraints, however, has not been forthcoming, partly because little experimental work has been done to address the formation of LPO in lower mantle materials.

Based on a bulk chemical composition model for the upper mantle (the pyrolite model), the lower mantle should consist of approximately 70% Mg-perovskite $(Mg,Fe)SiO_3$, approximately 20–25% magnesiowüstite (Mg,Fe)O, and less than 10% Ca-perovskite, $CaSiO_3$ (Ringwood, 1991). New experimental evidence suggests that Mg-perovskite undergoes a phase change to a post-perovskite phase at approximately 115–125 GPa (Murakami et al., 2004; Oganov and Ono, 2004; Shim et al., 2004). Thus, the dominant phase in the D″ layer may well be post-perovskite instead of perovskite. The question of which phase(s) are most likely to contribute to LPO-induced anisotropy becomes important. Karato (1998a) argued that (Mg,Fe)O is likely to be more elastically anisotropic at D″ conditions than perovskite (see also Wentzcovitch et al., 1998), although both magnesiowüstite and perovskite are probably anisotropic at these conditions (Isaak et al., 1989; Karki et al., 1997a,b). Additionally, the creep strength of magnesiowüstite in the lower mantle is probably much smaller than that of perovskite (Yamazaki and Karato, 2001) and lower mantle deformation may tend to be partitioned into (Mg,Fe)O, the weaker phase. Therefore, the development of LPO in (Mg,Fe)O during simple shear deformation, probably the dominant geometry at the base of the mantle, could be very important for generating seis-

mic anisotropy in D″. However, it is important to keep in mind that LPO in post-perovskite may also play a role in generating D″ anisotropy, and new experimental and theoretical results should shed light on the relative importance of post-perovskite and magnesiowüstite.

The importance of LPO in magnesiowüstite as a possible mechanism for generating seismic anisotropy in the lowermost mantle was first pointed out by Karato (1998a,b), but at this time little experimental work had addressed the development of fabric in (Mg,Fe)O. Stretton et al. (2001) investigated the mechanical behavior and resulting LPO of $(Mg_{0.8},Fe_{0.2})O$ using uniaxial compression tests, and found that significant LPO develops. Simple shear deformation experiments were first performed by Yamazaki and Karato (2002), who carried out a preliminary investigation of LPO development in $(Mg_{0.75},Fe_{0.25})O$ and FeO aggregates deformed in the dislocation creep regime. The deformation of the MgO endmember was investigated by Merkel et al. (2002) at pressures of the lower mantle, although their experiments were carried out at ambient temperature. Shear deformation experiments on $(Mg_{0.8},Fe_{0.2})O$ using a torsional configuration to very high strains (as large as $\gamma = 15.5$) were carried out by Heidelbach et al. (2003). Although several studies in the past few years have addressed the development of LPO in magnesiowüstite of various compositions, the effect of iron content on LPO has not yet been investigated systematically. In the work reported here, an extension of that of Yamazaki and Karato (2002), we performed simple shear deformation experiments of MgO, FeO, and three intermediate compositions at several homologous temperatures ($T/T_{melting}$). The goal of this study is to investigate the effects of composition and homologous temperature on LPO development and to apply the experimental results to the problem of anisotropic structure in the lowermost mantle.

2. Experimental procedure

2.1. Sample preparation

Samples were synthesized from powders of oxide reagents. MgO and Fe_2O_3 powders were mechanically mixed and ground in molar ratios yielding the desired compositions (MgO, $(Mg_{0.75},Fe_{0.25})O$, $(Mg_{0.50},Fe_{0.50})O$, $(Mg_{0.25},Fe_{0.75})O$, and FeO). For all compositions except the MgO endmember, powders were then put into a furnace in an alumina crucible at 1273 K for ~8–2 h with a CO_2/H_2 gas mixture to buffer oxygen fugacity within the wüstite stability field. After heating, the powders were re-mixed and re-heated at least once to achieve nearly complete reaction. The MgO powder and the conditioned (Mg,Fe)O and FeO powders were then cold-pressed using a split die into an iron jacket with a uniaxial pressure of ~20 MPa. The cold-pressed samples were isostatically hot-pressed in a gas-medium (Paterson) apparatus at 1473 K and 300 MPa for 200 min. During hot-pressing, the oxygen fugacity was buffered by the iron jacket. An optical micrograph of $(Mg_{0.50},Fe_{0.50})O$ starting material is shown in Fig. 1. Because grain growth is slower in MgO than FeO, starting grain sizes for pure MgO (~3–5 μm) were much smaller than that for the intermediate compositions (~30–70 μm). Although the starting grain size for FeO was not observed due to a pressure vessel leak early in the initial hot-press, we suppose it to be large, as the grain size of FeO deformed at 1473 K approached 300–400 μm. Except for FeO, the compositions of all starting materials were analyzed on a microprobe to ensure that an (Mg,Fe)O solid solution had been formed, that the correct molar ratios had been achieved, and that no contamination from the alumina crucibles occurred.

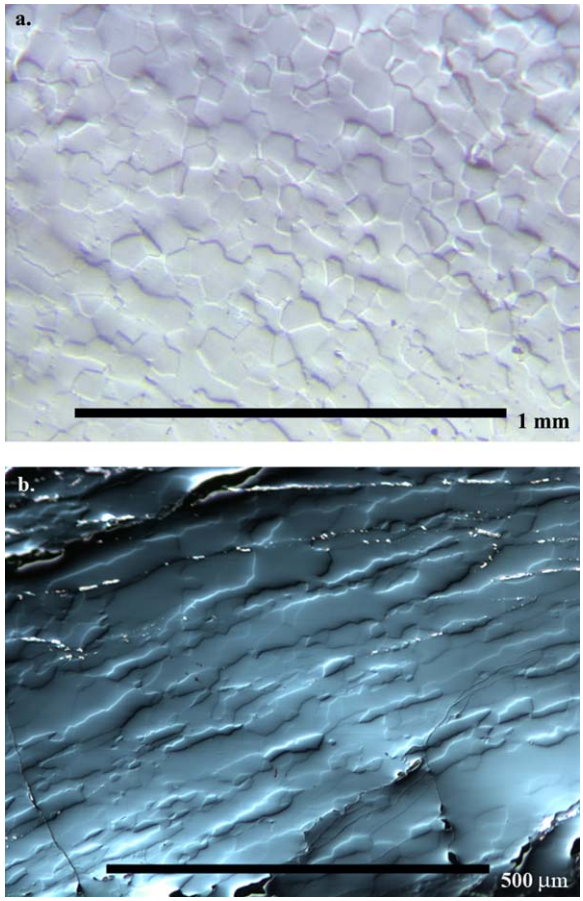

Fig. 1. Optical micrographs of undeformed $(Mg_{0.50},Fe_{0.50})O$ starting material (a) and FeO sample after deformation at 1273 K (b).

Table 1
Experimental conditions and LPO measurement results for six deformation experiments

Sample number	Composition	Temperature (K)	Shear strain (γ)	No. of grains measured	Starting grain size (μm)
MDL02	MgO	1473	4.2	1953	5
MDL03	(Mg.50,Fe.50)O	1473	4.5	518	30
MDL05	(Mg.75,Fe.25)O	1473	3.5	1757	45
MDL07	(Mg.25,Fe.75)O	1473	3.7	2055	70
MDL08a	FeO	1473	3.8	155	~150
MDL08b	FeO	1273	4.1	827	80

2.2. Deformation experiments

Slices ~1 mm thick were cut at an angle of 45° to the long axis from each of the cylindrical hot-pressed mixtures. For two of the experiments, the slices were then cut in half parallel to their thinnest dimension, and a strain marker of 0.1 mm-thick molybdenum foil was inserted. The sample was then sandwiched between two thoriated tungsten deformation pistons, cut at 45°. The surfaces of the deformation pistons had 40 μm deep grooves, spaced ~100–200 μm apart, to prevent slip at the sample–piston interface. The pistons and sample were put into an iron jacket and shear deformation was achieved by the uniaxial compression of alumina and zirconia pistons. A summary of the conditions for each deformation experiment is shown in Table 1, and a schematic diagram of the setup for the deformation experiments is shown in Fig. 2.

Deformation experiments were carried out on all compositions in a gas-medium Paterson apparatus at 1473 K and confining pressure of 300 MPa. One additional experiment was carried out on a FeO sample at 1273 K. For each experiment, the pressure was raised to ~220–235 MPa, and then the temperature was raised at a rate of 1.5 K/s, resulting in a final pressure of 300 MPa. After the desired pressure and temperature conditions were reached, the sample was annealed for one hour to obtain good contact between the sample and pistons. All experiments were carried out at a constant axial displacement rate of 0.0118 mm/min, and all experiments achieved a total strain of $\gamma = 3.5$–4.5 (corresponding to 3.5–4.5 mm of shear displacement for a 1 mm thick sample). We compared our experimental conditions (starting grain size, temperature, strain rate, and shear stress) with the deformation mechanism maps in Frost and Ashby (1982) and Karato (1998b), and all experimental conditions should fall within the dislocation creep regime. The large amount of total shear strain should ensure that the LPO pattern has reached a nearly steady state; although Heidelbach et al. (2003) showed that larger strains are needed to obtain truly steady-state fabrics in (Mg,Fe)O, Yamazaki and Karato (2002) showed that fabrics and the resulting anisotropy change very little after strains of $\gamma = 4$–5.

2.3. Microstructural observations

After deformation, the samples and pistons were cut into two halves parallel to the shear direction and perpendicular to the shear plane. Samples were polished with progressively smaller grit sizes, ending with 0.1 μm diamond paste and Syton colloidal silica solution. LPO

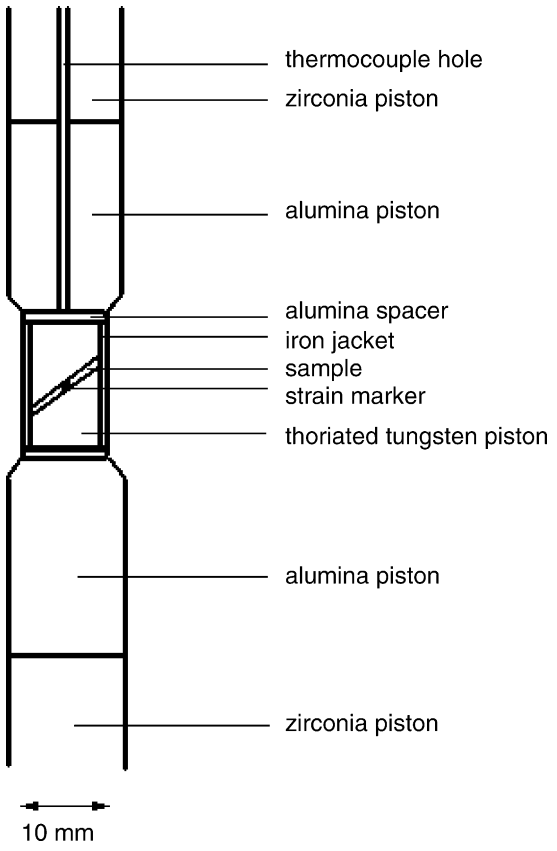

Fig. 2. Schematic diagram of sample assembly for deformation experiments.

was measured using the electron backscatter diffraction method (EBSD) (Dingley and Randle, 1992) on a scanning electron microscope (SEM). EBSD measurements were made on a Phillips XL30 SEM at Yale University. For five of the six samples, crystal orientations were determined in automatic beam scanning mode (Wright, 2000) with a step size slightly bigger than the average grain size. For the FeO sample deformed at 1473 K, the large grain size made automatic scanning impossible, and the orientation of every grain in the sample was measured and indexed manually. The deformed samples were also examined with an optical microscope and rotation and elongation of grains consistent with the sense of shear were observed. An optical micrograph of a deformed FeO sample (deformed at 1273 K) is shown in Fig. 1.

3. Results

3.1. Mechanical data

We converted the raw force and displacement data into stress–strain curves and measured the steady-state stress as a function of homologous temperature. It is important to note that mechanical data from shear deformation experiments are subject to large uncertainties due to the effects of heterogeneous deformation, change in sample thickness, etc. The measured force was converted into stress by dividing by the sample area and the change in sample area with increasing strain was taken into account in this calculation. The measured displacements were converted into strain using the previously measured stiffness of the Paterson apparatus (61.5 kN/mm in compression). Additionally, we apply a correction for the stiffness of the iron jacket by estimating the cross-sectional area of the iron jacket for each experiment and using published data for the strength of metallic iron (Frost and Ashby, 1982). A plot of log(σ) versus homologous temperature T/T_m is shown in Fig. 3.

A comparison of the stress/temperature curve in Fig. 3 with the deformation mechanism maps for MgO in Frost and Ashby (1982) for various grain sizes (initial grain sizes in our experiments ranged from ~5 μm to perhaps 150 μm, see Table 1) confirms that our experimental conditions should lie in the dislocation or power-law creep regime. Deformation in the dislocation creep regime should be governed by the relation

$$\frac{d\varepsilon}{dt} = A\sigma^n \exp\left(\frac{-Q}{RT}\right),$$

where ε is the strain, σ the stress, n represents the stress exponent, T the temperature, and A and β are the constants (see Evans and Kohlstedt, 1995, for an overview of the dislocation creep constitutive relations). All of our experiments were done at a constant temperature of 1473 K (with one exception) and at a constant strain rate. However, because of the dramatically different melting temperatures of the MgO and FeO endmembers, we covered a range of homologous temperatures ($T/T_{melting}$). The above equation predicts a linear relationship between log(stress) and the homologous temperature, which is what we observe in Fig. 3. Because the curve in Fig. 3 does not flatten, there is no indication that there is a change in deformation mechanism at different homologous temperatures. Dislocation creep is, of course, also indicated by our observations of strong lattice preferred orientation during our experiments (see below).

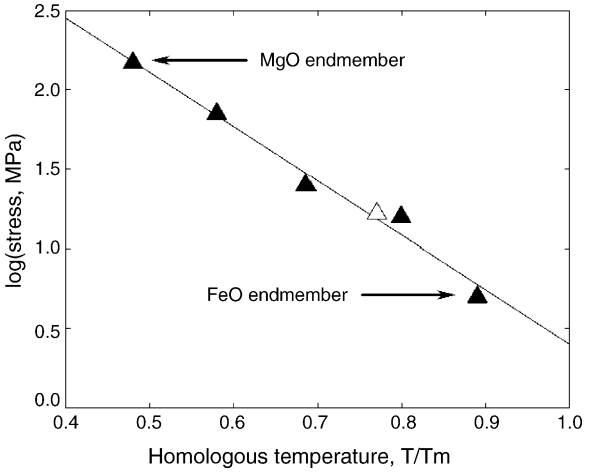

Fig. 3. Mechanical data from deformation experiments. We plot the log of the steady-state stress in MPa vs. the homologous temperature ($T/T_{melting}$). The line represents the best linear fit to this relation. Black triangles represent deformation experiments at 1473 K; the white triangle represents the experiment on FeO at 1273 K.

3.2. Microstructural observations

In Fig. 4, a dot map showing all measured crystal orientations for the [0 0 1], [0 1 1], and [1 1 1] axes of the MgO sample is shown, along with the corresponding pole figure plot of the calculated texture. The texture is represented by smoothing the individual orientation measurements with a Gaussian function with a 15° half-width. Pole figures for all six samples are shown in Fig. 5. For MgO, the observed texture is quite distinctive, with the [0 0 1] directions concentrated roughly in the direction of shear, in the shear plane perpendicular to the direction of shear, and orthogonal to the shear plane. However, the areas of [0 0 1] concentration paral-

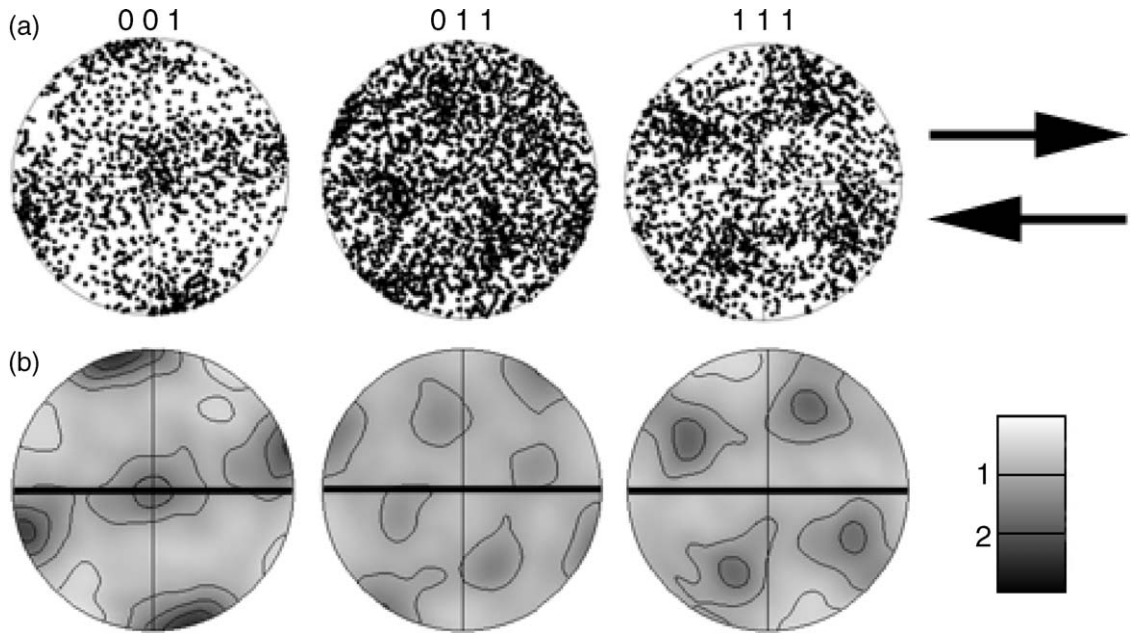

Fig. 4. Comparison of dot maps (a) and calculated pole figures (b) for the MgO sample. Dot maps show the lower-hemisphere projection of measured Euler angles for each grain (for the [0 0 1], [0 1 1], and [1 1 1] orientations, respectively). The pole figure representation is obtained using a Gaussian smoothing function with a 15° half-width. The shear plane corresponds to the E–W direction and is shown by the thick black lines on (b). The sense of shear is top to right (dextral) and is shown by the arrows at upper right. Pole figure density is represented by the grayscale and the maximum (black) corresponds to three multiples of uniform density (see scale bar at lower right). Projections are equal-area.

lel to the shear direction and orthogonal to the shear plane are tilted by ∼15–20°, a feature that had also been observed in other materials such as olivine (e.g. Zhang and Karato, 1995). This tilt can be observed for all samples except FeO. The pole figures for the [0 1 1] and [1 1 1] crystallographic directions also show distinctive areas of high concentrations. The observed fabric for $(Mg_{0.75},Fe_{0.25})O$ is quite similar to that of MgO, although the alignment of the [0 1 1] and [1 1 1] directions in $(Mg_{0.75},Fe_{0.25})O$ is less strong than for MgO. However, there is an interesting transition in fabric from $(Mg_{0.75},Fe_{0.25})O$ to $(Mg_{0.50},Fe_{0.50})O$. For the 50% Fe composition, the concentration of the [0 0 1] axis appears to be spread over larger areas. Additionally, there is no longer a peak in [0 0 1] concentration in the shear direction or contained in the shear plane, but perpendicular to the shear direction. Instead, these two orthogonal directions of [0 0 1] axes appear to be shifted in their plane by about 45°. For the $(Mg_{0.25},Fe_{0.75})O$ composition, a peak in the [0 0 1] axis concentration can still be seen roughly orthogonal to the shear plane (tilted ∼15–20°), but the concentrations in the shear plane appear more spread out than for the other compositions. The [0 0 1] concentrations for the FeO endmember samples lack the distinctive 15–20° tilt that was found for the other four compositions; for these samples, [0 0 1] concentrations lie either perpendicular to the shear plane, or in the shear plane at two orthogonal directions 45° from the shear direction, as for the $(Mg_{0.50},Fe_{0.50})O$ sample. (We note, however, that the FeO (1473 K) sample has only 155 measured grains, far fewer than the other five samples. This may be approaching the lower limit for number of grains needed to assure that the texture has been adequately statistically sampled.)

3.3. Seismic anisotropy

In order to translate the LPOs measured in this study into seismic anisotropy, several simplifying assumptions must be made. In the following calculations, we use the measured LPOs along with the single crystal elastic constants and density for MgO at 125 GPa (a typical pressure for D″) calculated by Karki et al. (1997a). This study and similar studies (Karki et al., 1997b, 1999; Karki and Stixrude, 1999; Wentzcovitch et al., 1998) use a first-principles calculation based on density functional theory to obtain the equation of state and elastic constants for MgO at pressures unattainable in the laboratory. The use of MgO elastic constants calculated for a pressure of 125 GPa and ambient temperature (rather than a temperature characteristic of D″) ignores the effects

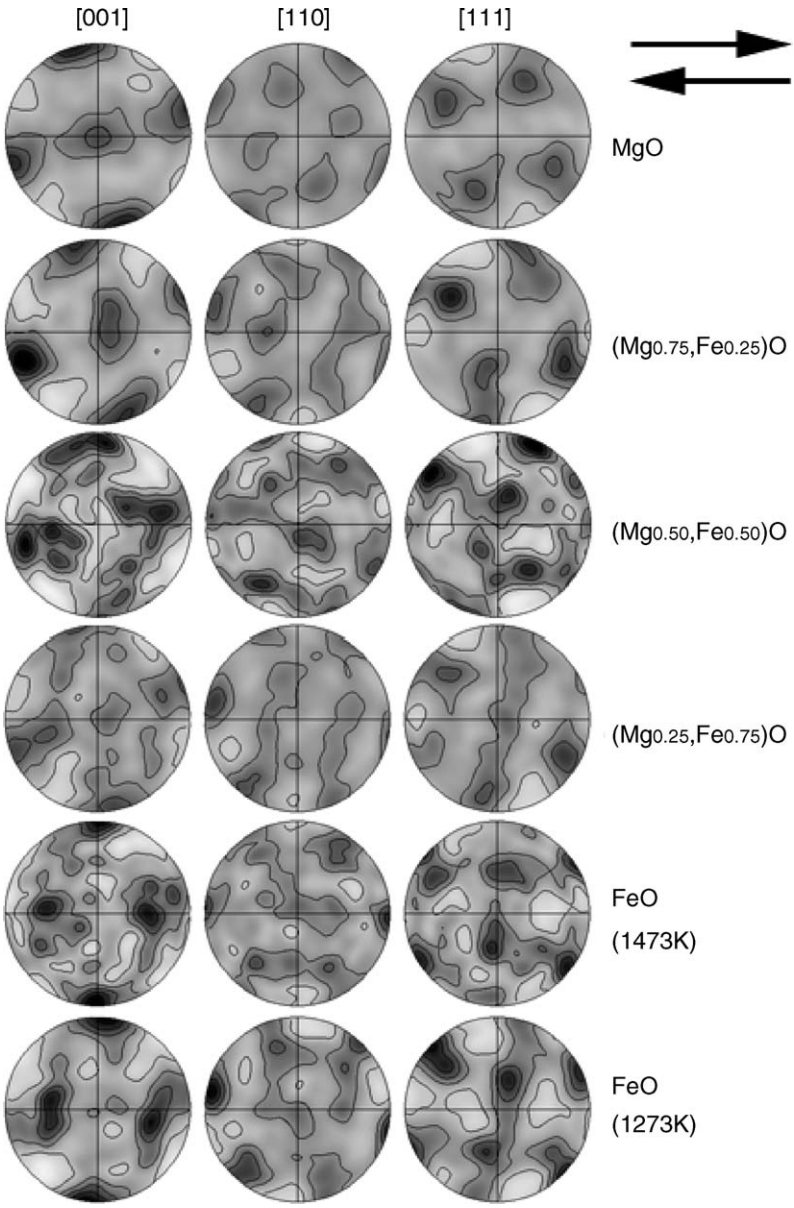

Fig. 5. Pole figures for the [0 0 1], [0 1 1], and [1 1 1] crystallographic orientations for six samples. Fe content increases from top (MgO) to bottom (FeO). As in this figure, the E–W direction corresponds to the shear plane and the sense of shear is dextral. The grayscale is the same as in Fig. 4; it is uniform for each sample, and the maximum value corresponds to three multiples of uniform density.

of temperature on elasticity; however, these effects are much smaller than those due to pressure. According to Yamazaki and Karato (2002), the effects of temperature between 0 and 4000 K at 140 GPa should modify the anisotropy by less than 10% (see also Stixrude, 2000, and Liebermann and Li, 1998); the effects of temperature are therefore ignored in this calculation.

We also use the MgO elastic constants for all five compositions, as the elastic constants of (Mg,Fe)O and FeO at lower mantle pressures have not been investigated. We note that significant differences in elastic constants with differing compositions have been observed for single crystal (Mg,Fe)O at ambient conditions, especially for Fe-rich compositions (Jacobsen et al., 2002); in fact, pure wüstite is elastically isotropic at ambient pressures. It is quite likely that the elasticity of Fe-rich magnesiowüstite at lower mantle pressures is significantly different than that of the MgO endmember, and we emphasize that our use of elastic constants for MgO is a significant simplification. However, the details of pressure effects on

elasticity in magnesiowüstite are not well known. A transition in spin state in (Mg,Fe)O at lower mantle pressures has been proposed (Badro et al., 2003; Sturhahn et al., 2005); this would likely modify the elasticity, but it is not known how. Given the large uncertainty in the effects of Fe at lower mantle conditions, we believe that the best approach is to use the better-known elastic constants for pure MgO at 125 GPa for our calculations. Subsequent work on the effects of Fe on elasticity at high pressures should allow for more accurate calculations in the future.

Bulk elastic constants C_{ij} from the measured LPOs were calculated using an algorithm by Mainprice (1990). (The notation C_{ij} uses the convention of contracting the fourth-rank elastic tensor c_{ijkl} into a 6×6 matrix C_{ij}, taking advantage of the symmetry properties of c_{ijkl}.) The Voigt–Reuss–Hill averaging scheme was used; this approach takes the arithmetic mean of the Voigt (assumes homogenous strain) and Reuss (assumes homogenous stress) averaging schemes. Calculated bulk elastic constants, along with single-crystal MgO constants, are shown in Table 2; all values are given in GPa. From the calculated elastic constants (quasi-) P and S wave velocities may be calculated by solving the Christoffel equation. This equation if given by:

$$\det |T_{ik} - \delta_{ik} V^2| = 0,$$

where δ_{ik} is the Kronecker delta function, V is one of three seismic velocities, and T_{ik} is the Christoffel stiffness matrix, given by

$$T_{ik} = c_{ijkl} X_j X_i,$$

where X_i and X_j are the direction cosines for the direction of interest. This equation is most easily solved by finding the eigenvalues of T_{ik}; this is the approach that the program by Mainprice (1990) takes. We solve for quasi-*P*, quasi-*S1*, and quasi-*S2* velocities over a range of propagation directions. Additionally, the strength of the S wave anisotropy A, given by

$$A = \max \left[\frac{|V_{S1} - V_{S2}|}{V_{S2}} \right] \times 100,$$

is calculated, along with the direction of the fast shear wave polarization.

The predicted pattern of anisotropy for single-crystal MgO is shown in Fig. 6. As Fig. 6 demonstrates, MgO is highly anisotropic at lower mantle pressures. Single crystal MgO has a *P* velocity anisotropy of 19.9% and a maximum *S* velocity anisotropy of 48.1%. The characteristics of shear wave anisotropy along with predicted fast shear wave polarization calculated from the measured LPOs for all six samples are shown in Fig. 7.

Table 2
Calculated bulk elastic constants in GPa for six samples, based on measured LPOs and single-crystal MgO elastic constants at 125 GPa from Karki et al. (1997a)

	C11	C12	C13	C14	C15	C16	C22	C23	C24	C25	C26	C33	C34	C35	C36	C44	C45	C46	C55	C56	C66
Single	1302	276	276	0	0	0	1302	276	0	0	0	1302	0	0	0	190	0	0	190	0	190
MgO	1035	411	407	0	1	28	1021	422	0	1	−23	1025	0	−2	−3	286	−3	1	268	0	273
$Mg_{75}O$	1019	421	415	2	−3	39	1014	419	−17	9	−36	1021	16	−6	−3	279	−3	10	275	1	284
$Mg_{50}O$	1031	400	422	−3	−11	32	1002	451	−1	7	−26	980	5	4	−6	312	−6	7	283	−4	264
$Mg_{25}O$	1014	420	420	4	1	−22	1001	433	−3	0	21	1000	−5	−1	1	293	0	0	280	3	281
FeO (high_*T*)	1039	405	410	6	4	−12	995	454	−14	−2	10	990	7	−2	2	315	2	−2	271	5	266
FeO (low_*T*)	1005	397	452	5	−9	8	1047	410	−7	−3	−4	992	2	12	−4	271	−5	−3	313	5	259

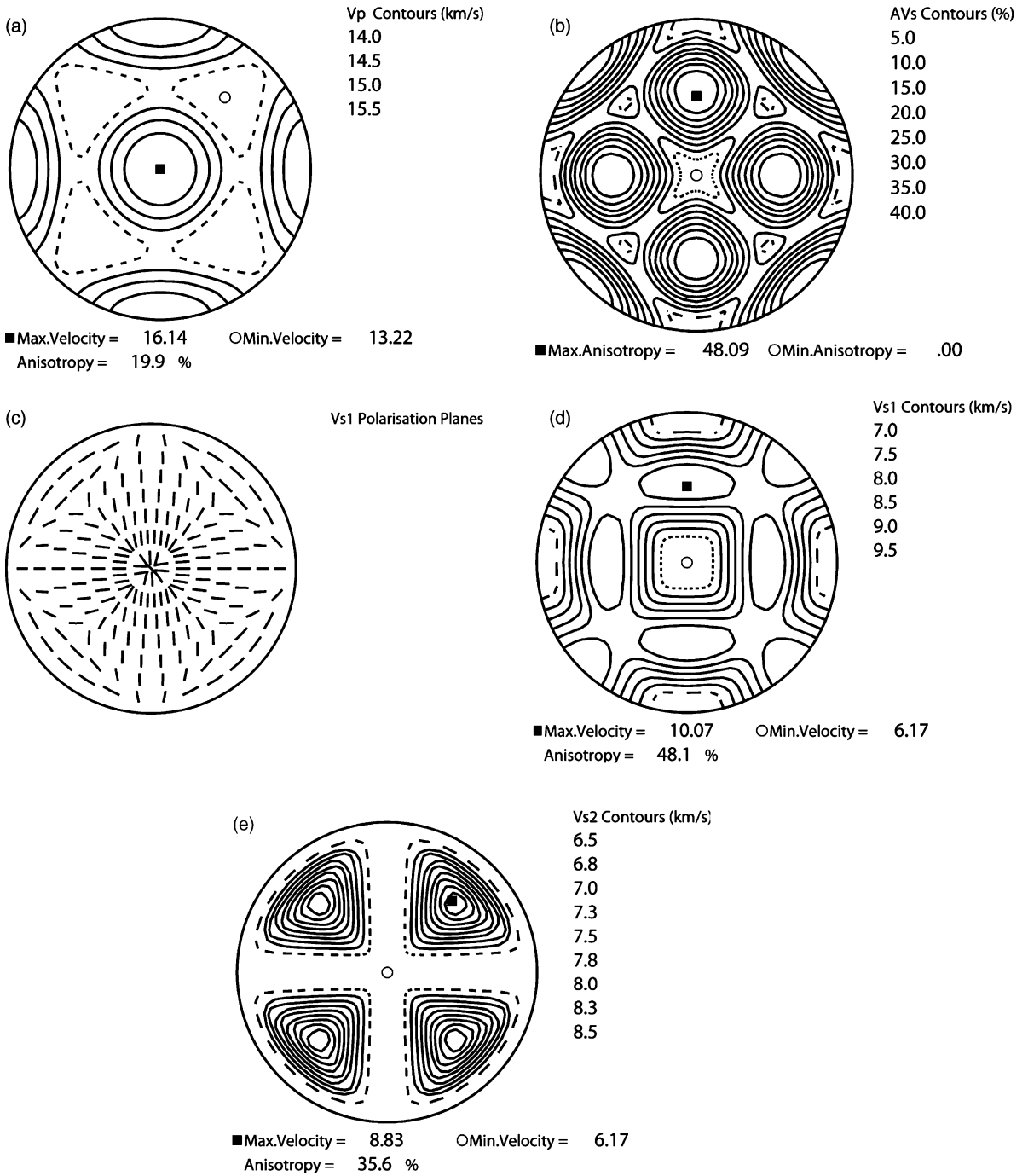

Fig. 6. Calculated anisotropy for single-crystal MgO at 125 GPa. Shown are contour plots of *P* wave velocity (a), S wave anisotropy (b), S1 polarization directions (c), S1 wave velocities (d), and S2 wave velocities (e). All plots are equal-area lower hemisphere projections.

The E–W direction for all plots in this figure represents the shear plane; for D″, we assume that the shear plane is horizontal. Fig. 7 demonstrates that composition can have a significant effect on the resulting anisotropy pattern, but also demonstrates that regardless of composition, the predicted patterns of anisotropy for (Mg,Fe)O have several features in common (see Section 4, below). The values of maximum calculated S anisotropy range from 5.0% to 11.6%, compared to the single crystal S anisotropy value of 48.1%.

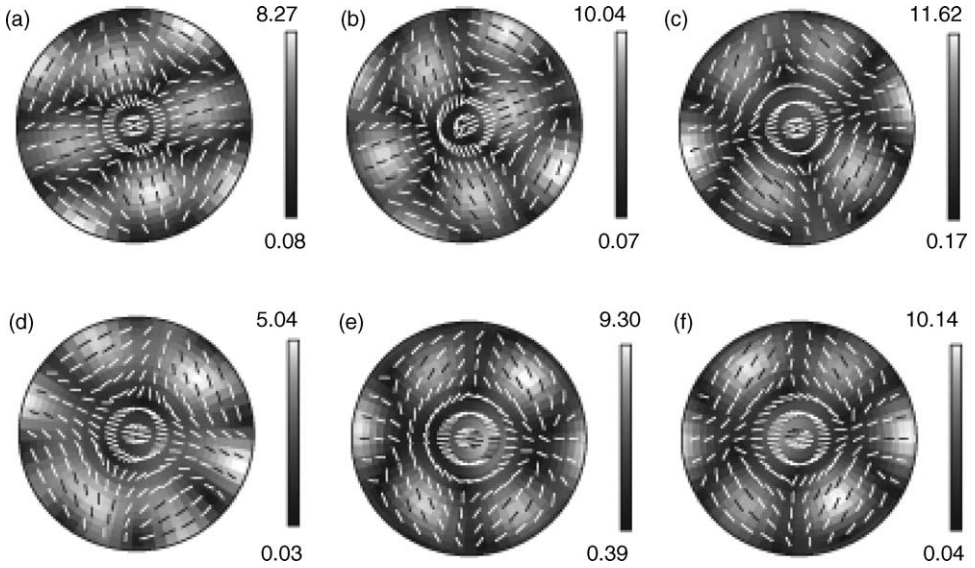

Fig. 7. Predicted shear wave splitting behavior based on the measured LPOs for six samples: MgO (a), Mg.75O (b), Mg.50O (c), Mg.25O (d), FeO at 1473 K (e), and FeO at 1273 K (f). The grayscale indicates the strength of S-wave anisotropy; the bars indicate the orientation of the fast splitting direction. Each scale bar is marked with the maximum (top) and minimum (bottom) value of S wave anisotropy, expressed as $A = \max[|V_{S1} - V_{S2}|/V_{S2}] \times 100$.

4. Discussion

4.1. Observed LPO

In this study, we observed changes in LPO pattern with increasing Fe content for (Mg,Fe)O samples. All experiments achieved a shear strain of $\gamma = 3.5$–4.5, which should insure that LPO has reached a nearly steady state. Because variables such as temperature, axial displacement rate, confining pressure, etc. were carefully controlled, we can attribute the difference in observed LPO for different samples to either: (1) effects of composition itself, or (2) effects of homologous temperature. All experiments in this study were performed at 1473 K (except for one additional FeO experiment at 1273 K), but because the melting temperatures of MgO and FeO are different (3099 K as opposed to 1650 K), this study covered a range of homologous temperatures ($T/T_{melting} = 0.48$–0.89). Because LPO is generated through dislocation creep, differences in fabric can be attributed to differences in the dominant slip systems for different materials, or to differences in the nature of grain-boundary migration.

As reviewed by Karato (1998a) and discussed by Stretton et al. (2001), Yamazaki and Karato (2002), Merkel et al. (2002), and Heidelbach et al. (2003), the Burgers vector, which represents the dominant slip direction, is always ⟨1 1 0⟩ for cubic NaCl-type crystal structures such as MgO. For NaCl, dislocation creep is dominated by glide on the {1 1 0} plane. However, the {1 0 0} and {1 1 1} glide planes could play an important role in deformation for NaCl-type materials, especially those with less ionic bonding than NaCl, such as MgO (Yamazaki and Karato, 2002). Karato (1998a) noted that temperature also affects the choice of glide planes, with glide on the {1 0 0} plane enhanced at higher temperatures because of the higher activation energy for the ⟨1 1 0⟩ {0 0 1} slip system. Because the relative importance of glide planes is affected both by temperature and by the degree of ionic bonding, further experiments (for example, holding the homologous temperature constant and varying the Fe content) may be needed to constrain the reasons for the differences in LPO observed in this study. However, the two experiments performed on FeO at different homologous temperatures ($T = 1473$ K and $T/T_m = 0.89$ versus $T = 1273$ K and $T/T_m = 0.77$) resulted in nearly identical LPO, which suggests that changes in observed LPO for (Mg,Fe)O may be primarily due to changes in composition. A part of the difference in fabrics among different compositions may be due to the difference in the degree to which the sample fabric has evolved. We note that although the fabric is nearly steady-state and there is little difference in seismic anisotropy beyond the shear strain of ∼4 as noted by Yamazaki and Karato (2002), there is some subtle development in fabric up to strain of ∼15 or so (Heidelbach et al., 2003). The fabrics of our more iron-rich samples resemble those at higher strains. It is possible that

the compositional dependence of fabric partly reflects the different degree of evolution of fabric among samples with different compositions. This is likely due to the fact that all kinetic processes occur faster for iron-rich samples than iron-poor counterparts compared at the same temperature and pressure. Further work is needed to separate the effects of composition and homologous temperature on LPO in magnesiowüstite and to definitively identify the slip systems that are active under different conditions, but we can use the range of LPOs observed in this study to make some general predictions about the possible style of anisotropy in the D″ layer.

We can compare our observed LPOs with those observed by previous studies. Specifically, the shear deformation experiments of Yamazaki and Karato (2002) and Heidelbach et al. (2003) are the most comparable to the work presented here. Although these studies examined a much narrower range of compositions than this work, we can compare our observed texture for $(Mg_{0.75},Fe_{0.25})O$ with observed LPOs for this composition from Yamazaki and Karato (2002) and with the intermediate-strain experiments on $(Mg_{0.8},Fe_{0.2})O$ from Heidelbach et al. (2003). While our observed textures (Fig. 5, second row from top) are not dramatically different from those of Yamazaki and Karato (2002) and Heidelbach et al. (2003), there are some differences in the details. These studies both observed a peak in the [1 1 0] crystallographic direction near the direction of shear. In our sample, this peak is much less well defined and it is shifted about 15–20° away from the shear direction, although we find that it is more prominent in the more Fe-rich samples. We also compare our observed LPOs for FeO (Fig. 5, bottom two rows) to the FeO experiment in Yamazaki and Karato (2002), although this earlier experiment was done at a lower temperature than ours (1073 K as opposed to 1273 and 1473 K). The distribution of orientations of the [1 1 0] and [1 1 1] crystallographic axes are quite similar to those observed by Yamazaki and Karato (2002), but the distributions of the [0 0 1] axes are somewhat different. However, the lack of dramatic differences in LPO between our FeO experiments and that of Yamazaki and Karato (2002) provides additional support for our hypothesis that the changes in LPO we observe in our different experiments are due to compositional effects rather than temperature effects.

4.2. Applications to anisotropy in D″

Can we apply the results of this laboratory study to the origin of D″ anisotropy? Before doing so, it is important to examine the assumptions that have been made. We must extrapolate the results of a study done in a laboratory to D″ conditions. The confining pressure used in these experiments was 300 MPa compared with ∼125 GPa at the base of the mantle; the experimental temperature was 1273–1473 K compared to temperatures of 2500–4000 K (Jeanloz and Williams, 1998); the laboratory strain rate of $\sim 3 \times 10^{-4}\,s^{-1}$ must be compared to mantle strain rates on the order of $\sim 10^{-14}$ to $10^{-16}\,s^{-1}$. As discussed earlier, several assumptions were made regarding the suitability of single crystal MgO elastic constants at 125 GPa for the anisotropy calculations.

However, if we assume that the LPOs due to dislocation creep observed in this study are comparable to the LPOs that would be generated due to dislocation creep at the conditions of the lowermost mantle, then we can compare the anisotropy patterns calculated in this study to seismological observations. These comparisons will allow us to assess the viability of the magnesiowüstite LPO model for anisotropy in D″. For the purpose of this argument, we assume that in at least come parts of D″, a transition from the diffusion creep that dominates the lower mantle to LPO-forming dislocation creep must occur. Karato (1998a) predicted that both the strain rate and the stresses should be higher at the boundary layers of the mantle such as D″, and that this effect should be enhanced for regions such as the circum-Pacific, where cold slab materials are possibly colliding with the CMB. Higher strain rates and higher stresses tend to favor dislocation creep over diffusion creep. Geodynamical models by McNamara et al. (2001, 2002) have demonstrated that dislocation creep may indeed be concentrated in the lowermost mantle for a downgoing slab model. We also emphasize that the range of compositions considered in this laboratory study may not all be directly applicable to the D″ layer; the range of iron content in the (Mg,Fe)O system at the base of the mantle is not well constrained (e.g. Mao et al., 1997). However, the range of LPOs observed in the (Mg,Fe)O system in this laboratory study is likely to be representative of the range of LPOs potentially formed in the lowermost mantle due to dislocation creep of magnesiowüstite. Finally, we point out that newly discovered stable phase of $MgSiO_3$ near the conditions of the D″ layer (Murakami et al., 2004) is probably also elastically anisotropic (Tsuchiya et al., 2004). Consequently, a combined effect of anisotropic structure of (Mg,Fe)O and post-perovskite may be responsible for seismic anisotropy near the bottom of the lower mantle. However, the nature of LPO in the post-perovskite phase is not well known, which hampers a detailed assessment of the combined effect of both phases. Oganov et al. (2005) presented a theoretical study of possible slip

systems, but their results do not agree with the results of an experimental study on analog material, $CaIrO_3$ (Miyajima et al., 2005).

As summarized by Kendall (2000) and Lay et al. (1998), the main features of D″ anisotropy that have been observed are as follows. First, there is a general lack of splitting, or total splitting of less than 0.3 s, of near-vertically propagating *SKS*-type phases. Second, in the circum-Pacific region, core-diffracted or pre-diffracted shear phases that traverse roughly horizontal paths through D″ are significantly split (up to ∼10 s), with *SH* arriving before *SV*, indicating $V_{SH} > V_{SV}$ anisotropy with a vertical symmetry axis (transverse isotropy). Third, beneath the central Pacific, anisotropy is highly spatially variable, with some evidence for $V_{SV} > V_{SH}$ anisotropy and azimuthal anisotropy. Are the predicted anisotropy patterns found in this study consistent with these observations? We examine the plots in Fig. 7 of calculated S anisotropy and fast shear wave polarizations. In these figures, the E–W direction represents the shear plane, which is considered to be horizontal for D″. Most of the predicted anisotropy patterns are consistent with a small amount of splitting of vertically propagating *SKS*-type phases. For the two most Mg-rich samples, no *SKS* splitting is predicted; however, the measured LPO for the FeO samples does predict some splitting of vertically propagating phases. For the remaining two compositions, little splitting is predicted for strictly vertical paths but some splitting is predicted for phases that deviate more significantly from the vertical, such as *SKKS*. The predicted anisotropy for horizontally propagating shear waves is also consistent with the observation that shear wave splitting with $V_{SH} > V_{SV}$ occurs in the circum-Pacific. For all anisotropy patterns, *S* phases propagating in the shear plane (that is, horizontally) should be significantly split at certain azimuths. The pattern of azimuthal anisotropy in the shear plane, however, is different for different compositions. While no $V_{SV} > V_{SH}$ anisotropy is predicted from the LPOs observed in this study, it may be that $V_{SV} > V_{SH}$ anisotropy in the central Pacific region of D″ is generated through a mechanism other than the one examined in this study. The central Pacific is presumably a site of mantle upwelling and the arguments for the localization of dislocation creep may not hold in this region.

Because the patterns of anisotropy calculated from the measured LPOs in this study agree well with most seismological observations of D″ anisotropy, LPO of magnesiowüstite seems to be a viable mechanism for generating anisotropic structure in D″. However, the SPO hypothesis that D″ anisotropy is the result of horizontal layering or oriented inclusions also agrees with the seismological observations discussed above (Kendall and Silver, 1998a). Can the observations of LPO in this study be used to distinguish between the LPO and the SPO models of D″ anisotropy? One testable difference between the two models is the prediction from this study that LPO-generated fabric will result in azimuthal anisotropy in the horizontal plane, while most SPO configurations will not. The splitting of horizontally propagating *S* phases traversing D″ should depend on the direction of propagation if the LPO hypothesis is correct. Azimuthal anisotropy has not been well constrained due to the difficulty of finding suitable source/receiver combinations for a variety of backazimuths, but a recent waveform modeling study by Garnero et al. (2004) found evidence for azimuthal anisotropy in the D″ region beneath the Caribbean. Hall et al. (2004) pointed out that differential splitting of *SKS* and *SKKS* phases may be used to constrain D″ anisotropy, and noted that LPO-based mechanisms should generate azimuthal variations in splitting, which is consistent with our results. Further studies on azimuthal anisotropy in D″ using waveform modeling, differential *SKS*/*SKKS* splitting, or innovative source/receiver geometries may help to differentiate between the LPO and SPO models.

5. Conclusions

We have performed shear deformation experiments in the dislocation creep regime on (Mg,Fe)O aggregates over a range of compositions and homologous temperatures. We find that LPO develops at large strains for all samples, but the style of LPO changes with increasing Fe content. Using the measured LPO patterns and single crystal elastic constants for MgO at lowermost mantle pressures, we calculate bulk elastic constants C_{ij} and resulting patterns of anisotropy for all samples. The predicted patterns of anisotropy are generally consistent with the main features of seismological observations of D″ in the circum-Pacific region, including small amounts of splitting of vertical *SKS*-type phases and splitting of horizontally propagating *S* phases due to $V_{SH} > V_{SV}$ anisotropy. Measured LPOs in (Mg,Fe)O would predict azimuthal anisotropy in the horizontal (shear) plane, however, while most SPO-based models do not. The investigation of azimuthal anisotropy in D″, which has not been well constrained, should provide a means to distinguish between LPO- and SPO-generated anisotropy. Additionally, if strain-induced LPO of (Mg,Fe)O is the cause of anisotropy in D″, the characterization of its azimuthal anisotropy may provide constraints on the composition and/or melting temperature of (Mg,Fe)O in the lowermost mantle.

Acknowledgements

The authors thank Tim Grove, Steve Singletary, Jessica Warren, and Mark Zimmerman for technical advice and assistance. The paper was greatly improved by the thoughtful and helpful comments of two anonymous reviewers, and we thank them for their efforts. This research was supported by the National Science Foundation through grants to S.-i. K. and B. E. (OCE-0452787) and through a Graduate Research Fellowship to M.D.L.

References

Badro, J., Fiquet, G., Guyot, F., Rueff, J.-P., Struzhkin, V.V., Vankó, G., Monaco, G., 2003. Iron partitioning in Earth's mantle: toward a deep lower mantle discontinuity. Science 300, 789–791.

Cormier, V.F., 1986. Synthesis of body waves in transversely isotropic earth models. Bull. Seismol. Soc. Am. 76, 231–240.

Dingley, D.J., Randle, V., 1992. Microstructural determination by electron backscattered diffraction. J. Mater. Sci. 27, 4545–4566.

Doornbos, D.J., Spilopoulos, S., Stacey, F.D., 1986. Seismological properties of D″ and the structure of the thermal boundary layer. Phys. Earth Planet. Inter. 41, 225–239.

Evans, B., Kohlstedt, D.L., 1995. Rheology of rocks. In: Ahrens, T.J. (Ed.), Rock Physics and Phase Relations. Am. Geophys. Union, AGU Ref. Shelf, vol. 3.

Fouch, M.J., Fischer, K.M., Wysession, M.E., 2001. Lowermost mantle anisotropy beneath the Pacific; imaging the source of the Hawaiian Plume. Earth Planet. Sci. Lett. 190, 167–180.

Frost, H.J., Ashby, M.F., 1982. Deformation Mechanism Maps. Pergamon Press, Oxford, UK.

Garnero, E.J., Lay, T., 1997. Lateral variations in lowermost mantle shear wave anisotropy beneath the North Pacific and Alaska. J. Geophys. Res. 102, 8121–8135.

Garnero, E.J., Lay, T., 2003. D″ shear velocity heterogeneity, anisotropy, and discontinuity structure beneath the Caribbean and Central America. Phys. Earth Planet. Inter. 140, 219–242.

Garnero, E.J., Maupin, V., Lay, T., Fouch, M.J., 2004. Variable azimuthal anisotropy in Earth's lowermost mantle. Science 306, 259–261.

Hall, S.A., Kendall, J.-M., van der Baan, M., 2004. Some comments on the effects of lower-mantle anisotropy on SKS and SKKS phases. Phys. Earth Planet. Inter. 146, 469–481.

Heidelbach, F., Stretton, I., Langenhorst, F., Mackwell, S., 2003. Fabric evolution during high shear strain deformation of magnesiowüstite ($Mg_{0.8}$,$Fe_{0.2}$)O. J. Geophys. Res. 108, 2154, doi:10.1029/2001JB001632.

Isaak, D.G., Anderson, O.L., Goto, T., 1989. Measured elastic moduli of single-crystal MgO up to 1800 K. Phys. Chem. Miner. 16, 704–713.

Jacobsen, S.D., Reichmann, H.J., Spetzler, H.A., Mackwell, S.J., Smyth, J.R., Angel, R.J., McCammon, C.A., 2002. Structure and elasticity of single-crystal (Mg,Fe)O and a new method of generating shear waves for gigahertz ultrasonic interferometry. J. Geophys. Res. 107, doi:10.1029/2001JB000490.

Jeanloz, R., Williams, Q., 1998. The core–mantle boundary region. Rev. Mineral. 37, 241–259.

Karato, S.-i., 1989. Defects and plastic deformation in olivine. In: Karato, S.-i., Toriumi, M. (Eds.), Rheology of Solids and of the Earth. Oxford University Press, Oxford, UK.

Karato, S.-i., 1998a. Some remarks on the origin of seismic anisotropy in the D″ layer. Earth Planets Space 50, 1019–1028.

Karato, S.-i., 1998b. Seismic anisotropy in the deep mantle, boundary layers and the geometry of mantle convection. Pure Appl. Geophys. 151, 565–587.

Karato, S.-i., Zhang, S., Wenk, H.-R., 1995. Superplasticity in Earth's lower mantle: evidence from seismic anisotropy and rock physics. Science 270, 458–461.

Karki, B.B., Stixrude, L., 1999. Seismic velocities of major silicate and oxide phases of the lower mantle. J. Geophys. Res. 104, 13025–13033.

Karki, B.B., Stixrude, L., Clark, S.J., Warren, M.C., Ackland, G.J., Crain, J., 1997a. Structure and elasticity of MgO at high pressure. Am. Miner. 82, 51–60.

Karki, B.B., Stixrude, L., Clark, S.J., Warren, M.C., Ackland, G.J., Crain, J., 1997b. Elastic properties of orthorhombic $MgSiO_3$ perovskite at lower mantle pressures. Am. Miner. 82, 635–639.

Karki, B.B., Wentzcovitch, R.M., de Gironcoli, S., Baroni, S., 1999. First-principles determination of elastic anisotropy and wave velocities of MgO at lower mantle conditions. Science 286, 1705–1707.

Kendall, J.-M., 2000. Seismic anisotropy in the boundary layers of the mantle. In: Karato, S.-i., et al. (Ed.), Earth's Deep Interior: Mineral Physics and Tomography from the Atomic to the Global Scale, Am. Geophys. Union, Geophys. Monogr. Ser., vol. 117.

Kendall, J.-M., Silver, P.G., 1996. Constraints from seismic anisotropy on the nature of the lowermost mantle. Nature 381, 409–412.

Kendall, J.-M., Silver, P.G., 1998. Investigating causes of D″ anisotropy. In: Gurnis, M., et al. (Ed.), The Core-Mantle Boundary Region. Am. Geophys. Union, Geodyn. Ser., vol. 28.

Lay, T., Williams, Q., Garnero, E., Kellogg, L., Wysession, M.E., 1998. Seismic wave anisotropy in the D″ region and its implications. In: Gurnis, M., et al. (Ed.), The Core-Mantle Boundary Region. Am. Geophys. Union, Geodyn. Ser., vol. 28.

Lay, T., Young, C.J., 1991. Analysis of seismic SV-waves in the core's penumbra. Geophys. Res. Lett. 18, 1373–1376.

Liebermann, R.C., Li, B., 1998. Elasticity at high pressures and temperatures. Rev. Mineral. 37, 459–492.

Mainprice, D., 1990. An efficient Fortran program to calculate seismic anisotropy from the lattice preferred orientation of minerals. Comput. Geosci. 16, 385–393.

Mao, H., Shen, G., Hemley, R.J., 1997. Multivariable dependence of Fe–Mg partitioning in the lower mantle. Science 278, 2098–2100.

Matzel, E., Sen, M.K., Grand, S.P., 1996. Evidence for anisotropy in the deep mantle beneath Alaska. Geophys. Res. Lett. 23, 2417–2420.

McNamara, A.K., Karato, S.-i., van Keken, P.E., 2001. Localization of dislocation creep in the lower mantle: implications for the origin of seismic anisotropy. Earth Planet. Sci. Lett. 191, 85–99.

McNamara, A.K., van Keken, P.E., Karato, S.-i., 2002. Development of anisotropic structure in the Earth's lower mantle by solid-state convection. Nature 416, 310–314.

Meade, C., Silver, P.G., Kaneshima, S., 1995. Laboratory and seismological observations of lower mantle isotropy. Geophys. Res. Lett. 22, 1293–1296.

Merkel, S., Wenk, H.-R., Shu, J., Shen, G., Gillet, P., Mao, H.-k., Helmley, R.J., 2002. Deformation of polycrystalline MgO at pressures of the lower mantle. J. Geophys. Res. 107, 2271, doi:10.1029/2001JB000920.

Mitchell, B.J., Helmberger, D.V., 1973. Shear velocities at the base of the mantle from observations of S and ScS. J. Geophys. Res. 78, 6009–6020.

Miyajima, N., Ohgushi, K., Ichihara, M., Yagi, T., Frost, D., Rubie, D.C., 2005. Crystal morphology and dislocation textures of the $CaIrO_3$ phase—TEM study of an analogue of the post-perovskite phase. Eos Trans. AGU 86 (52), Fall Meet. Suppl., Abstract MR23B-0069.

Moore, M.M., Garnero, E.J., Lay, T., Williams, Q., 2004. Shear wave splitting and waveform complexity for lowermost mantle structures with low-velocity lamellae and transverse isotropy. J. Geophys. Res. 109, doi:10.1029/2003JB002546.

Murakami, M., Hirose, K., Kawamura, K., Sata, N., Ohishi, Y., 2004. Post-perovskite phase transition in $MgSiO_3$. Science 304, 855–858.

Oganov, A.R., Martonak, R., Laio, A., Raiteri, P., Parrinello, M., 2005. Anisotropy of Earth's D″ layer and stacking faults in the $MgSiO_3$ post-perovskite phase. Nature 438, 1142–1144.

Oganov, A.R., Ono, S., 2004. Theoretical and experimental evidence for a post-perovskite phase of $MgSiO_3$ in Earth's D″ layer. Nature 430, 445–448.

Ringwood, A.E., 1991. Phase transitions and their bearing on the constitution and dynamics of the mantle. Geochim. Cosmochim. Acta 55, 2083–2110.

Ritsema, J., 2000. Evidence for shear velocity anisotropy in the lowermost mantle beneath the Indian Ocean. Geophys. Res. Lett. 27, 1041–1044.

Russell, S.A., Lay, T., Garnero, E., 1998. Seismic evidence for small-scale dynamics in the lowermost mantle at the root of the Hawaiian hotspot. Nature 396, 255–258.

Shim, S.-H., Duffy, T.S., Jeanloz, R., Shen, G., 2004. Stability and crystal structure of $MgSiO_3$ perovskite to the core-mantle boundary. Geophys. Res. Lett. 31, doi:10.1029/2004GL019639.

Stixrude, L., 2000. Elasticity of mantle phases at high pressure and temperature. In: Karato, S.-i., et al. (Ed.), Earth's Deep Interior: Mineral Physics and Tomography from the Atomic to the Global Scale. Am. Geophys. Union, Geophys. Monograph Ser., vol. 117.

Stretton, I., Heidelbach, F., Mackwell, S., Langenhorst, F., 2001. Dislocation creep of magnesiowüstite ($Mg_{0.8}Fe_{0.2}O$). Earth Planet. Sci. Lett. 194, 229–240.

Sturhahn, W., Jackson, J.M., Lin, J.-F., 2005. The spin state of iron in minerals of Earth's lower mantle. Geophys. Res. Lett. 32, doi:10.1029/2005GL022802.

Tsuchiya, T., Tsuchiya, J., Umemoto, K., Wentzcovitch, R.M., 2004. Elasticity of post-perovskite $MgSiO_3$. Geophys. Res. Lett. 31, doi:10.1029/2004GL020278.

Vinnik, L., Farra, V., Romanowicz, B., 1989. Observational evidence for diffracted S_V in the shadow of the Earth's core. Geophys. Res. Lett. 16, 519–522.

Vinnik, L., Bréger, L., Romanowicz, B., 1998. On the inversion of Sd particle motion for seismic anisotropy in D″. Geophys. Res. Lett. 25, 679–682.

Vinnik, L., Romanowicz, B., Le Stunff, Y., Makeyeva, L., 1995. Seismic anisotropy in the D″ layer. Geophys. Res. Lett. 22, 1657–1660.

Wentzcovitch, R.M., Karki, B.B., Karato, S., Da Silva, C.R.S., 1998. High pressure elastic anisotropy of $MgSiO_3$ perovskite and geophysical implications. Earth Planet. Sci. Lett. 164, 371–378.

Wright, S.I., 2000. Fundamentals of automated EBSD. In: Schwartz, A.J. (Ed.), Electron Backscatter Diffraction in Materials Science. Kluwer Academic/Plenum Publishers, New York, USA.

Wysession, M.E., Lay, T., Revenaugh, J., Williams, Q., Garnero, E.J., Jeanloz, R., Kellogg, L.H., 1998. The D″ discontinuity and its implications. In: Gurnis, M., et al. (Ed.), The Core-Mantle Boundary Region. Am. Geophys. Union, Geodyn. Ser., vol. 28.

Yamazaki, D., Karato, S.-i., 2001. Some mineral physics constraints on the rheology and geothermal structure of Earth's lower mantle. Am. Miner. 86, 385–391.

Yamazaki, D., Karato, S.-i., 2002. Fabric development in (Mg,Fe)O during large strain, shear deformation: implications for seismic anisotropy in Earth's lower mantle. Phys. Earth Planet. Int. 131, 251–267.

Zhang, S., Karato, S.-i., 1995. Lattice preferred orientation of olivine aggregates deformed in simple shear. Nature 375, 774–777.